Journal of Non-Crystalline Solids 459 (2017) 26–31

Contents lists available at ScienceDirect

Journal of Non-Crystalline Solids

journal homepage: www.elsevier.com/locate/jnoncrysol

Enhanced tensile ductility of metallic glass matrix composites with novel microstructure

Yunpeng Jiang [a,*], Longgang Sun [b], Qingqing Wu [b], Kun Qiu [b]

[a] State Key Laboratory of Mechanics and Control of Mechanical, Nanjing University of Aeronautics and Astronautics, Nanjing 210016, China
[b] Department of Engineering Mechanics, Hohai University, Nanjing 210098, China

ARTICLE INFO

Article history:
Received 15 October 2016
Received in revised form 3 December 2016
Accepted 26 December 2016
Available online 2 January 2017

Keywords:
Metallic glass
Tensile plasticity
Microstructure
Finite element method (FEM)

ABSTRACT

In this paper, numerical study was conducted to reveal the effects of particle concentration and particle morphology on the tensile behaviors of metallic glass (MG) matrix composites. Free volume acts as an internal state variable to depict the nucleation, growth and coalescence of shear bands in the MG matrix composites on the basis of free volume theory, which was incorporated into the ABAQUS code as a user material subroutine UMAT. The impedance efficiency of various microstructures on the propagation of shear bands was discussed, and whereby a novel network configuration of second-phase was suggested to improve MG's tensile plasticity. The present work is helpful to understand the failure mechanisms and the tensile toughening design of MG matrix composites.

1. Introduction

In order to overcome the intrinsic brittleness of metallic glasses (MGs), introducing second-phase in the MG matrix to make the heterogeneous composites is the most effective measure [1]. Up to date, some inorganic powders, such as SiC, SiO_2, Mg, Mo and graphite powders, were dispersed in the Mg-, Zr-, and Ti based MGs to make *ex-situ* composites [2–3]; and many kinds of *in-situ* composites were directly synthesized [4–5]. In general, these MG matrix composites exhibit better compressive plasticity as compared to the pure MG matrix. However, the tensile ductility was improved a little, even not enhanced in most of the cases. However, Hofmann pointed out that MG matrix composites have the potential capability of marked tensile ductility and ultra-high toughness [6]. Qiao et al. [7] synthesized the $Ti_{46}Zr_{20}V_{12}Cu_5Be_{17}$ MG matrix composite, containing 43% volume fractioned dendrites, and 8.0% plastic elongation was successfully achieved. Wu et al. [8] developed a MG composite with large tensile ductility and work-hardening ability by using the 'transformation-induced plasticity' concept to amorphous alloys. Zhai et al. [9] introduced Sn element in a $Ti_{47}Zr_{25}Nb_6Cu_5Be_{17}$ MG matrix composite, and effectively suppressed the strain-induced work-softening effect by MG matrix. Finally, the largest ductility of ~10% was reached. As the particle concentration exceeded a critical value of 40%, a large plasticity was gained [10]. The deformation asymmetry associated with glass plasticity is alleviated as the particle volume fraction rises. Wu et al. [11] investigated the tensile behavior of ZrCu-based MG composites with various crystalline volume fractions. A tensile plastic strain of more than 10% was obtained in a MG matrix composite with a crystalline loading of 32.6%.

To better enhance the tensile plasticity of MGs, a better understanding of the tensile mechanism in MG matrix composites should be an important prerequisite. Based on the free volume theory, Jiang et al. [12–13] conducted the parameter analyses on the roles of particle volume fraction, particle shape, particle orientation and particle yielding strength in the enhancement of the tensile ductility for MG matrix composites. Shete et al. [14] performed finite strain continuum FEM to reflect the role played by the volume fraction and strain hardening behavior of crystalline particles on the strength and ductility of the composites. Balch et al. [15] performed *in-situ* diffraction testing to measure strains in crystalline particles of MG matrix composites. Even though a marked tensile plasticity was gain, but the strain softening stage usually appears in most of MG matrix composites. In the real composites, many microstructure parameters are interplayed, and the individual effect of each factor is hard to be given and reflected with the real composite measurement.

In this work, free volume theory is adopted to characterize the shear band evolution in the MG matrix, and then effect of particle concentration and morphology on the tensile behaviors of MG matrix composites is studied. With increasing particle concentration, particles will form an interconnecting network morphology, and effectively restrict the free propagation of shear bands in the MG matrix. Motivated by the shear banding mechanism in highly compacted particles filled MG matrix composite, a composite with a novel network microstructure is advanced, and the corresponding toughening mechanisms in such novel composites is revealed. The toughening efficiency by this morphology is compared with discrete particles filled composites.

* Corresponding author.
E-mail address: ypjiang@nuaa.edu.cn (Y. Jiang).

http://dx.doi.org/10.1016/j.jnoncrysol.2016.12.033
0022-3093/

2. Constitutive relations of MG

The shear-band initiation, growth, and propagation form the fundamental deformation mechanism in MGs. At the microscopic scale, shear-band formation is believed to be associated with the evolution of the local structural order. One atomistic mechanism capturing shear-band formation and evolution in MGs is the free volume theory developed by Spaepen [16] and further extended by Steif [17]. From a continuum mechanics point of view, the shear-band is a result of strain softening and considered to be a strain localization phenomenon. The free volume model regards free volume as an internal state variable, which controls the structural evolution at the atomic level in MGs.

According to the J_2-type, small strain visco-plasticity framework [18], the free volume theory is extended to a multi-axial stress state. The strain rate is decomposed into the elastic and plastic parts

$$\dot{\varepsilon}_{ij} = \dot{\varepsilon}^e_{ij} + \dot{\varepsilon}^p_{ij} \tag{1}$$

The above elastic part is expressed by the general Hooke's law:

$$\dot{\varepsilon}^e_{ij} = \frac{1+\nu}{E}\left(\dot{\sigma}_{ij} - \frac{\nu}{1+\nu}\dot{\sigma}_{kk}\delta_{ij}\right) \tag{2}$$

with a characteristic time scale $t^* = tf^{-1}\exp(\Delta G^m / k_B T)$, where f denotes the frequency of atomic vibration, E is elastic modulus, ν is Poisson's ratio, ΔG^m is the activation energy, k_B is the Boltzmann constant, and T is the absolute temperature. Based on the normalized time t^*, the equations are differentiated in terms of the normalized time scale t^*. The plastic part is rewritten as [19]:

$$\dot{\varepsilon}^p_{ij} = \exp\left(-\frac{1}{\nu_f}\right)\sinh\left(\frac{\sigma_e}{\sigma_0}\right)\frac{S_{ij}}{\sigma_e} \tag{3}$$

where ν_f denotes the average free volume per atom, $\sigma_0 = 2k_BT/\Omega$ is the reference stress, $S_{ij} = \sigma_{ij} - \sigma_{kk}\delta_{ij}/3$ is the deviatoric stress tensor, and $\sigma_e = (S_{ij}S_{ij})^{1/2}$ is the von Mises' stress. It should be noting that a dot over a quantity X denotes $(\dot{X}) = f^{-1}\exp(\Delta G^m / k_B T)(\partial X / \partial t)$, which is used in the following expression. The free volume evolution equation in the multi-axial stress state is expressed as:

$$\dot{\nu}_f = \frac{1}{\alpha}\exp\left(-\frac{1}{\nu_f}\right)\left\{\frac{3(1-\nu)}{E}\left(\frac{\sigma_0}{\beta\nu_f}\right)\left(\cosh\left(\frac{\sigma_e}{\sigma_0}\right)-1\right) - \frac{1}{n_D}\right\} \tag{4}$$

where α stands for a geometric factor of order 1; $\sigma_0 = 2k_BT/\Omega$ is the reference stress, ν_f is the average free volume per atom, $\nu_f = \nu_f/\alpha\nu^*$ is the normalized free volume, $\beta = \nu^*/\Omega$, and n_D is the number of atomic jumps needed to annihilate a free volume equal to ν^*, and is usually taken to be 3– 10.

3. FEM simulation

The above constitutive equations are implemented into ABAQUS code with a user-defined material subroutine UMAT [20]. In this simulation, the shear band evolution is described by an *internal state variable*, *i.e.* the normalized free volume ν_f as given in Eq. (3). The initially undeformed numerical model of this sample as shown in Fig. 1 for particle filled composites in (a) and network composites (b). During the computation, all the nodes in the bottom node set are prevented from motion along axis-*x*. A positive displacement along axis-*x* is exerted to the single node located at the top-right corner with the desired test strain-rate. The multi-point constraint (MPC) equation is applied to the rest of the nodes along the top surface in order to keep their deformation coordinate with the top-right corner node. To suppress rigid-body motions of the sample, the node located at the bottom-left corner is also prevented from moving along axis-*y*. The remaining nodes in the bottom and top nodes are free to move along axis-*y*.

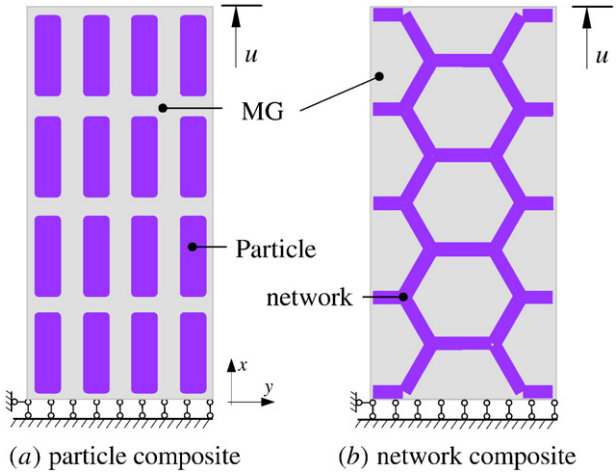

Fig. 1. Computational model adopted in ABAQUS package for 2D modeling of plane-strain tension and the corresponding boundary conditions exerted during the computation for particle filled composite (a) and for network composites (b).

In order to better reflect the shear localization in the MGs, some elements with a slightly lower value of initial free volume act as nucleation sites for shear banding. The initial free volume ν_0 was presumed to be statistically varied over the elements obeying a Gaussian distribution function with a mean value of 0.05, and a standard deviation of 0.005. The ductile particles should obey the following yielding principle,

$$\frac{\varepsilon_{eq}}{\varepsilon_y} = \left(\frac{\sigma_{eq}}{\sigma_y}\right)^{\frac{1}{N}} - 1, \sigma_{eq} \geq \sigma_y \tag{5}$$

where σ_y, σ_{eq}, ε_y and ε_{eq} are the yielding stress, von Mises's stress, yielding strain and equivalent strain, respectively. N is the strain hardening coefficient, and will be discussed by changing its value. The material properties for the MG matrix are: $E = 100$ GPa, $\nu = 0.38$, $n_D = 3$, $\alpha = 0.21$, $\beta = 1.0$ and $\sigma_0 = 94$ MPa. Those properties for the particle phase are [10]: $E = 150$ GPa, $\nu = 0.35$, $\varepsilon_y = 0.0067$ and $\sigma_y = 1.2$ GPa.

4. Results and discussion

4.1. Effect of particle concentration

Fig. 2 shows the stress–strain relation and the corresponding snapshots of shear banding formation for the MG matrix composites with different particle volume fraction under uniaxial tension, and strain hardening coefficient of ductile particle N = 0.1. With increasing particle volume fraction, the uniform plastic deformation of MG matrix composites becomes more and more evident. As compared to the unreinforced MG, the plastic deformations are increased after adding the ductile particles. The inherent micro-deformation mechanism is clearly illustrated by the associated snapshots of shear banding evolution. As the particle amount or particle thickness is small, the resistance to shear band propagation appears to be too low to effectively impede its father progression. Therefore, the plastic elongations are also not high, and only one main shear band form during the plastic deformation. But as $V_P = 45\%$, the particles become very dense, and thus the restriction to the shear banding also increases, leading to two main shear bands appear.

On the other hand, N = 0.1 means that the work hardening ability of ductile particle is not strong, which was also reflected in these contours. Some particles located in the shear banding path are distorted seriously, which fully indicates that the strength of particle phase is not high.

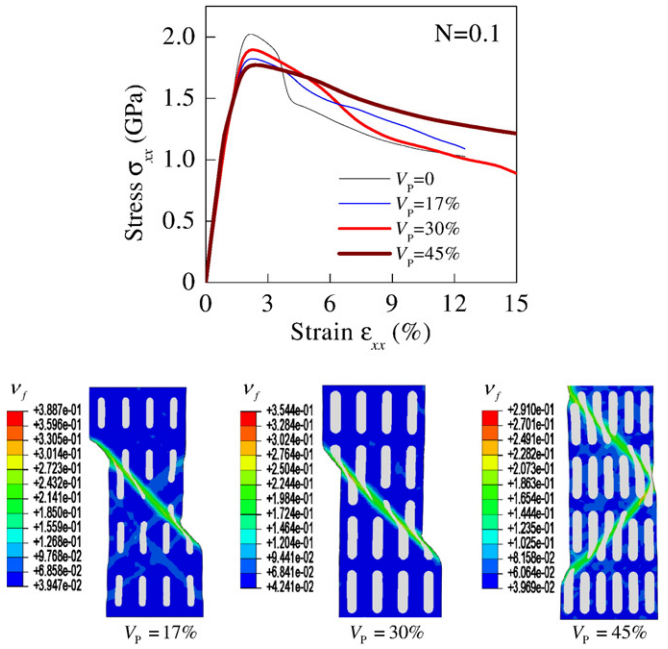

Fig. 2. The stress–strain relation and the corresponding snapshots of shear banding formation for the MG matrix composites with different particle volume fraction under uniaxial tension, and strain hardening coefficient of ductile particle N = 0.1.

Therefore, these particles with low strain hardening ability could not effectively hinder the propagation of the shear band.

4.2. Effect of strain hardening coefficient

Fig. 3 and Fig. 4 illustrate the effect of strain hardening coefficient on the enhancement in the tensile ductility of MG matrix composites. These results again confirm the dependence of tensile plasticity of MG matrix composites on the particle volume fraction as mentioned in Section 4.1. With increasing the strain hardening ability of particle phase, the shear bands have to deflect from the preceding route as they meet particles, instead of running through them, which indicates the particle strength is relatively high. As clearly seen from the contours in Fig. 3, the multiple shear bands appear in the composites with particle concentration 30%, and a nearly uniform deformation occur for the composite with particle loading 45%. As N = 0.3, almost no particles was sheared, even no serious deform happens. In summary, the strain hardening ability of particle has a significant effect on the shear band evolution and the corresponding plasticity. As shear band confronts the particle with high strain hardening capability, shear band should deviate, or round the particles as seen in Fig. 5. Therefore, the traveling distance enhances largely.

For the 45% composite as shown in Fig. 4, no shear bands seem to form anymore, which differs from the experimental observations. The difference between the present simulations and actual experimental observations mainly lies in the limitation of numerical model, which cannot embody the microstructure details in the real composites. It is expected that the real composites is really inhomogeneous, and an arbitrary minute impurity could induce the stress concentration effect, which results in the shear banding activation. On the other word, the present numerical model could not fully replicate the real microstructures due to the limited computing power.

4.3. Effect of particle number density

Fig. 6 presents the dependence of the stress–strain relations on the particle spacing and the resulting snapshots of shear band formation

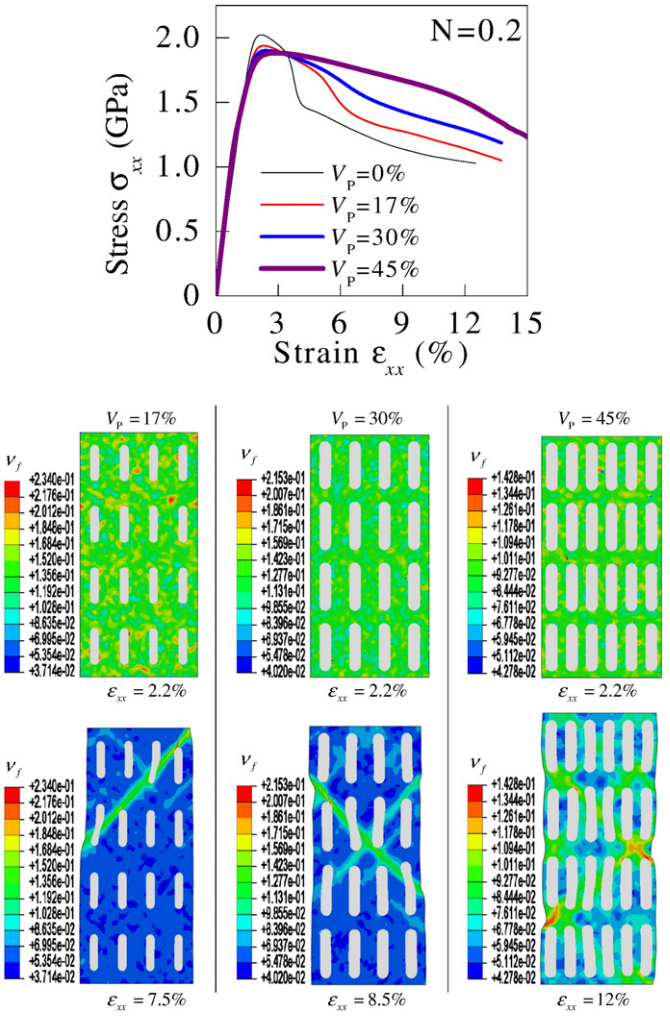

Fig. 3. The stress–strain relation and the corresponding snapshots of shear banding formation for the MG matrix composites with different particle volume fraction under uniaxial tension, and strain hardening coefficient of ductile particle N = 0.2.

at the tensile strain $\varepsilon_{xx} = 10\%$. At a given particle concentration $V_p = 17\%$, the composites with 12 and 20 particles shows different tensile plasticity, and MG matrix composite with more particles is much better in the plasticity. Only a main shear band happens in the composites with 12 particles, while multiple shear bands appear in the composite with 20 particles. The resulting big difference is mainly caused by the two following reasons: (1) After introducing many more particles, the local stress field should be more complicated, and consequently the probability to initiate a shear band also increases, which contributes to the formation of multiple shear bands and their intersection; (2) The spacing between particles decreases with increasing particle numbers or decreasing particle size, which indicates that many more particles may locate in the propagation path of shear banding. A representative volume element with N_p spherical particles is used to establish the quantitative relationship between the particle number and particle spacing. The dimension of RVE is a, and particle radius is r, then the particle spacing λ is expressed as

$$V_P = \frac{\pi r^2 N_P}{a^2} \tag{6}$$

$$\lambda = \left(\sqrt{\pi/V_P} - 2\right) r = \left(1 - 2\sqrt{\frac{V_P}{\pi}}\right)\sqrt{\frac{a^2}{N_P}} \tag{7}$$

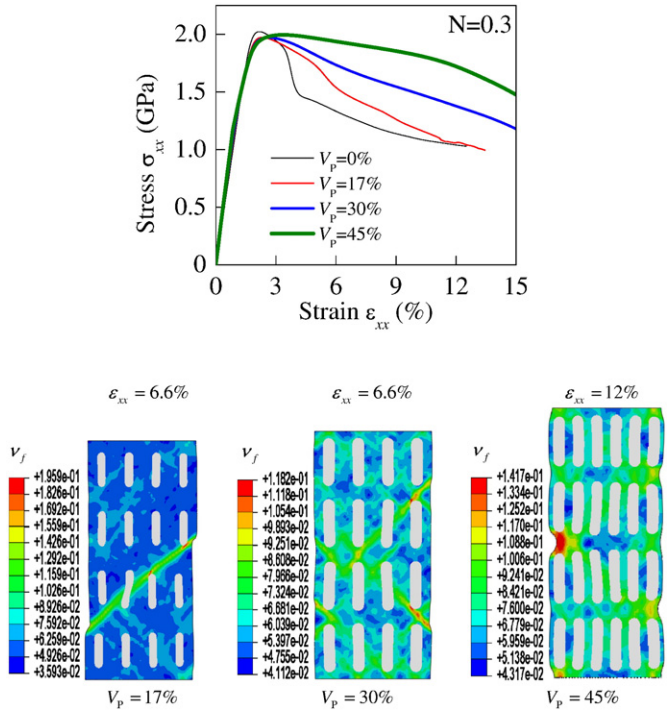

Fig. 4. The stress–strain relation and the corresponding snapshots of shear banding formation for the MG matrix with different particle volume fraction under uniaxial tension, and strain hardening coefficient of ductile particle N = 0.3.

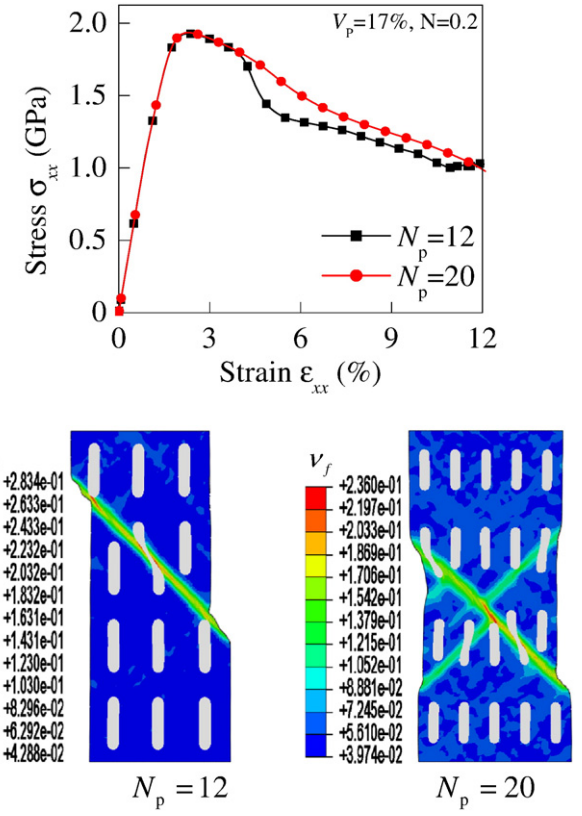

Fig. 6. Dependence of the stress–strain relations on the particle spacing and the corresponding snapshots of shear banding formation at the tensile strain $\varepsilon_{xx} = 10\%$.

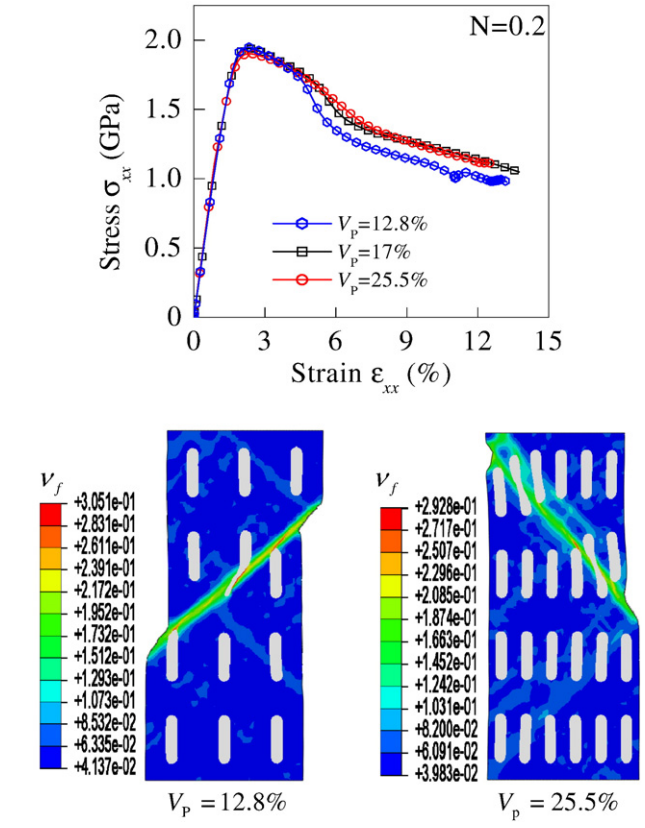

Fig. 5. Dependence of the stress–strain relations on the particle volume fractions and the corresponding snapshots of shear banding formation under uniaxial tension.

From the above equations, particle spacing should reduce with increasing particle numbers. Therefore, many more particles would appear in the shear banding path, and thus the resistance to their progression could be enhanced greatly.

4.4. Effect of network morphology

In the preceding simulations, the tensile plasticity improves evidently with increasing particle concentration. From the microstructure point of view, high volume fraction of particles can form a relatively condense network, which effectively hinder the propagation of shear banding. Motivated by this rule, we are attempting to introduce a web-like morphology second phase into the MG matrix and to form a composite system, which is called 'network composite'. As for the preparation of real network composites, some network microstructures, such as fiber mat, vegetable sponge and *etc.*, can be added in the MG matrix to make the composites.

Fig. 7 gives the comparison between the stress-strain relations of particle filled and network composites. The present modeling clearly confirmed the feasibility of adopting a novel network microstructure in improving the tensile ductility of MGs. The network morphology successfully divides the MG matrix into many isolated segments as shown in the associated contours, in which the mature shear bands are not easily to happen, and thus the collapse damage is avoided. As for the network second phase, the influence of interface separation would not be very important, since the network second phase should across over the whole sample, and thus the two phases share the applied loading through the whole deformation.

Moreover, the reliance of the mechanical performance of such composites on 'particle' volume fraction and strain hardening coefficient

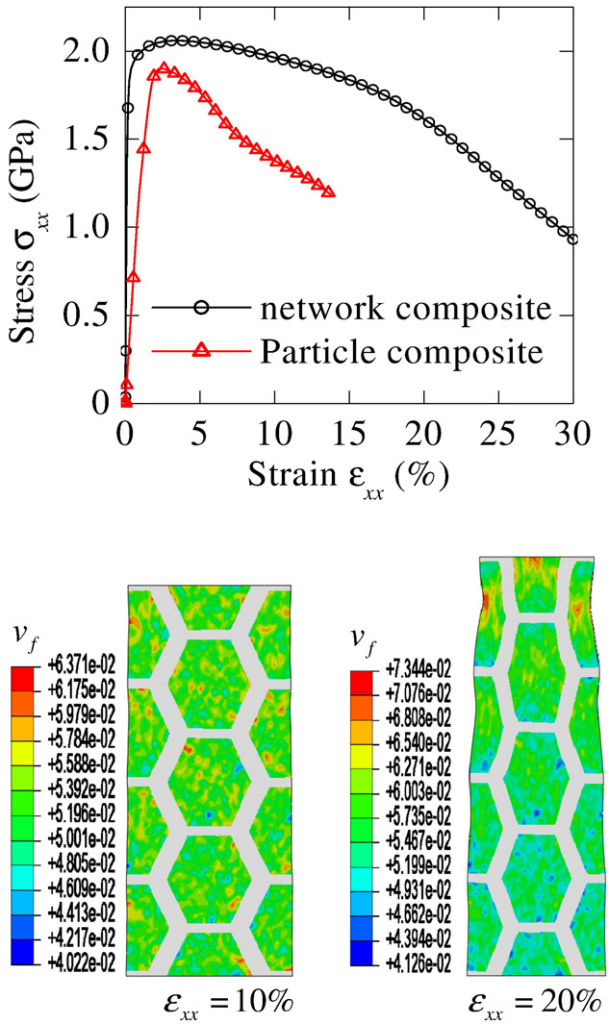

Fig. 7. Comparison between the stress-strain relations of particle filled and network composites (V_p = 30%, and N = 0.2), and the shear band evolution in network composite is associated.

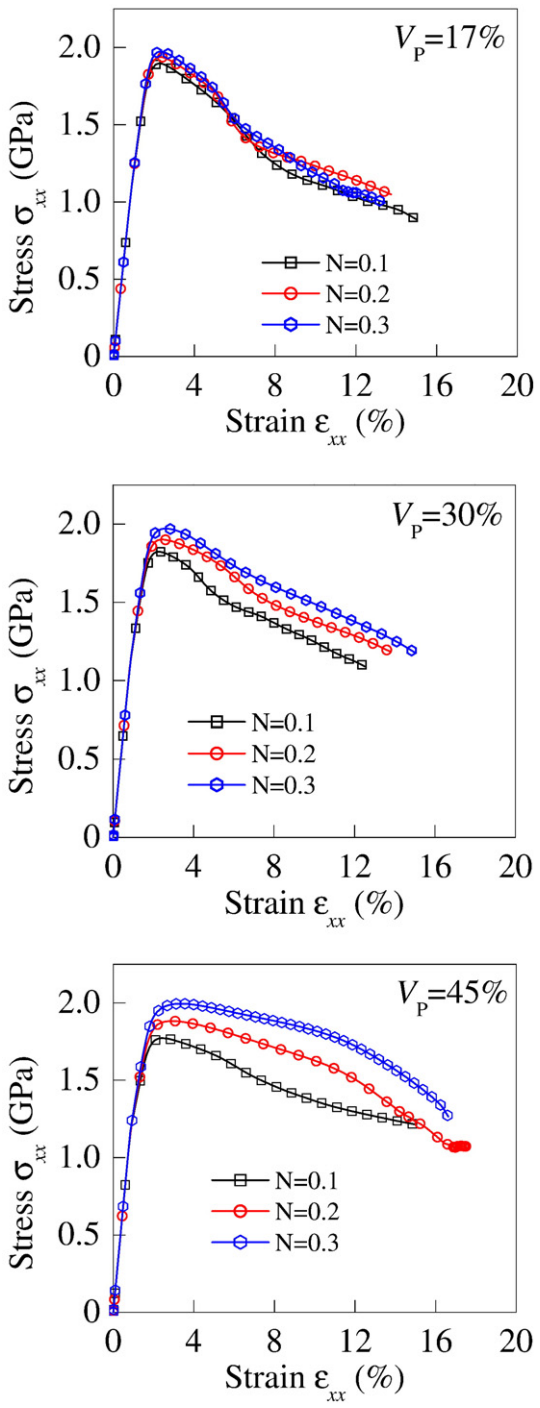

Fig. 8. Dependence of the stress–strain relations on the second-phase concentration and strain hardening coefficients for network composites.

was fatherly analyzed as shown in Fig. 8. The similar conclusions could be reached, the increase in the 'particle' volume fraction and the strain hardening coefficient can improve the tensile plasticity of MG matrix composites. The strong work hardening capability of particles could result in a big increase in the plasticity of composite, which is also confirmed by the experiment [21]. The Martensite transition and the resulting strain hardening effect are shown in Fig. 9, in which strong work hardening effect is very remarkable during the phase transition.

5. Conclusion

In this work, free volume theory-based FEM was referred to analyze the effect of particle concentration and particle morphology on the tensile behaviors of MG matrix composites. Discussing the shear banding in various microstructures could establish the dependence of tensile plasticity of MG matrix composites on the particle volume fraction and morphology. Several main conclusions are reached,

(1) Increasing particle concentration can effectively improve the tensile plasticity of MG matrix composites;
(2) Increasing strain hardening coefficient of particle phase is capable of enhancing the tensile plasticity of MG matrix composites;
(3) As compared to discrete particle filled composites, the network morphology of second-phase should be more efficient in improving the tensile plasticity of MG matrix composites.

Acknowledgement

This work was supported by the Fundamental Research Funds for the Central Universities (YAH16056), Jiangsu Provincial Natural Science Foundation (BK2012407) and Program for New Century Excellent Talents in University (NCET-12-0840).

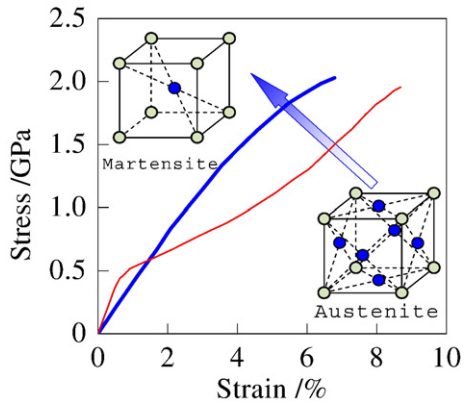

Fig. 9. Martensite transition and the resulting strain hardening effect.

References

[1] J.W. Qiao, H.L. Jia, P.K. Liaw, Mater. Sci. Eng. R 100 (2016) 1–69.
[2] J.S.C. Jang, T.H. Li, S.R. Jian, J.C. Huang, T.G. Nieh, Intermetallics 19 (2011) 738–743.
[3] M.E. Siegrist, J.F. Loffler, Scr. Mater. 56 (2007) 1079–1082.
[4] R.L. Narayan, P.S. Singh, D.C. Hofmann, N. Hutchinson, K.M. Flores, U. Ramamurty, Acta Mater. 60 (2012) 5089–5100.
[5] D.C. Hofmann, J.Y. Suh, A. Wiest, G. Duan, M.L. Lind, M.D. Demetriou, W.L. Johnson, Nature 451 (2008) 1085–1089.
[6] D.C. Hofmann, J.Y. Suh, A. Wiest, W. Johnson, Scr. Mater. 59 (2008) 684–687.
[7] J.W. Qiao, A.C. Sun, E.W. Huang, Y. Zhang, P.K. Liaw, C.P. Chuang, Acta Mater. 59 (2011) 4126–4137.
[8] Y. Wu, Y.H. Xiao, G.L. Chen, C.T. Liu, Z.P. Lu, Adv. Mater. 22 (2010) 2770–2773.
[9] H.M. Zhai, H.F. Wang, F. Liu, J. Alloys Compd. 685 (2016) 322–330.
[10] M.L. Lee, Y. Li, C.A. Schuh, Acta Mater. 52 (2004) 4121–4131.
[11] F.F. Wu, K.C. Chan, S.T. Li, G. Wang, J. Mater. Sci. 49 (2014) 2164–2170.
[12] Y.P. Jiang, K. Qiu, Mater. Des. 65 (2015) 410–416.
[13] Y.P. Jiang, X.P. Shi, K. Qiu, Mater. Des. 77 (2015) 32–40.
[14] M.K. Shete, I. Singh, R. Narasimhan, U. Ramamurty, Scr. Mater. 124 (2016) 51–55.
[15] D.K. Balch, E. Üstündag, D.C. Dunand, Metall. Mater. Trans. A 34 (2003) 1787–1797.
[16] F. Spaepen, Acta Metall. 25 (1977) 407–415.
[17] P.S. Steif, F. Spaepen, J.W. Hutchinson, Acta Metall. 30 (1982) 447–455.
[18] J.W. Hutchinson, Acta Mech. Sinica 28 (2012) 1078–1086.
[19] Y.F. Gao, Model. Simul. Mater. Sci. Eng. 14 (2006) 1329–1345.
[20] ABAQUS Theory Manual, HKS inc., 2010 510.
[21] R. Wei, Y. Chang, Y.F. Li, G. Li, S. Yang, C.J. Zhang, L. He, Mater. Sci. Eng. A 587 (2013) 233–239.